Surface plasmon photonic structures in terahertz quantum cascade lasers

Olivier Demichel[1], Lukas Mahler, Tonia Losco, Cosimo Mauro, Richard Green, Jihua Xu, Alessandro Tredicucci, and Fabio Beltram

NEST CNR-INFM and Scuola Normale Superiore
Piazza dei Cavalieri 7, I-56126 Pisa, Italy
[1] *Present address: École Normale Supérieure, 24 rue Lhomond, F-75005 Paris, France*
l.mahler@sns.it

Harvey E. Beere and David A. Ritchie

Cavendish Laboratory, University of Cambridge, Madingley Road, Cambridge CB3 0HE, United Kingdom

Vincas Tamošiūnas

Semiconductor Physics Institute, A. Goštauto Str. 11, LT-01108 Vilnius, Lithuania

Abstract: The periodic scattering of the surface plasmon modes employed in the waveguide of terahertz quantum cascade lasers is shown to be an efficient method to control the properties of the laser emission. The scatterers are realized as thin slits in the metal and top contact layer carrying the surface plasmon. This technique provides larger coupling strengths than previously reported and can be used in various device implementations. Here the method is applied to realize a distributed feedback resonator without back-facet reflection, to achieve vertical emission of the radiation with second-order gratings, and to increase the facet reflectivity by fabricating passive distributed Bragg reflectors.

OCIS codes: (140.3070) Infrared and far-infrared lasers; (140.3490) Lasers, distributed-feedback; (140.5960) Semiconductor lasers; (240.6680) Surface plasmons; (250.7270) Vertical emitting lasers.

References and links

1. W. L. Barnes, A. Dereux, and T. W. Ebbesen, "Surface plasmon subwavelength optics," Nature **424**, 824-830 (2003).
2. R. Köhler, A. Tredicucci, F. Beltram, H. E. Beere, E. H. Linfield, A. G. Davies, D. A. Ritchie, R. C. Iotti, and F. Rossi "Terahertz semiconductor-heterostructure laser," Nature **417**, 156-159 (2002).
3. B. Williams, S. Kumar, Q. Hu, and J. Reno "Operation of terahertz quantum-cascade lasers at 164 K in pulsed mode and at 117 K in continuous-wave mode," Opt. Express **13**, 3331-3339 (2005), http://www.opticsexpress.org/abstract.cfm?URI=OPEX-13-9-3331.
4. B. S. Williams, S. Kumar, Q. Hu, and J. L. Reno "High-power terahertz quantum cascade lasers," Electron. Lett. **42**, 89-91 (2006).
5. J. Darmo, V. Tamosiunas, G. Fasching, J. Kröll, K. Unterrainer, M. Beck, M. Giovannini, J. Faist, C. Kremser, and P. Debbage, "Imaging with a Terahertz quantum cascade laser," Opt. Express **12**, 1879-1884 (2004), http://www.opticsexpress.org/abstract.cfm?URI=OPEX-12-9-1879.
6. S. Barbieri, J. Alton, C. Baker, T. Lo, H. Beere, and D. Ritchie, "Imaging with THz quantum cascade lasers using a Schottky diode mixer," Opt. Express **13**, 6497-6503 (2005), http://www.opticsexpress.org/abstract.cfm?URI=OPEX-13-17-6497.
7. J. R. Gao, J. N. Hovenier, Z. Q. Yang, J. J. A. Baselmans, A. Baryshev, M. Hajenius, T. M. Klapwijk, A. J. L. Adam, T. O. Klaassen, B. S. Williams, S. Kumar, Q. Hu, and J. L. Reno, "Terahertz heterodyne receiver based on a quantum cascade laser and a superconducting bolometer," Appl. Phys. Lett. **86**, 244104 (2005).

#70268 - $15.00 USD Received 25 April 2006; revised 31 May 2006; accepted 31 May 2006

8. H. -W. Hübers, S. Pavlov, A. Semenov, R. Köhler, L. Mahler, A. Tredicucci, H. Beere, D. Ritchie, and E. Linfield, "Terahertz quantum cascade laser as local oscillator in a heterodyne receiver," Opt. Express **13**, 5890-5896 (2005), http://www.opticsexpress.org/abstract.cfm?URI=OPEX-13-15-5890.
9. L. Mahler, R. Köhler, A. Tredicucci, F. Beltram, H. E. Beere, E. H. Linfield, D. A. Ritchie, and A. G. Davies "Single-mode operation of terahertz quantum cascade lasers with distributed feedback resonators," Appl. Phys. Lett. **84**, 5446-5448 (2004).
10. L. Ajili, J. Faist, H. Beere, D. Ritchie, G. Davies, and E. Linfield "Loss-coupled distributed feedback far-infrared quantum cascade lasers," Electron. Lett. **41**, 419-421 (2005).
11. B. Williams, S. Kumar, Q. Hu, and J. Reno "Distributed-feedback terahertz quantum-cascade lasers with laterally corrugated metal waveguides," Opt. Lett. **30**, 2909-2911 (2005).
12. L. Mahler, A. Tredicucci, R. Köhler, H. E. Beere, E. H. Linfield, and D. A. Ritchie "High-performance operation of single-mode terahertz quantum cascade lasers," Appl. Phys. Lett. **87**, 181101 (2005).
13. C. Weeber, Y. Lacroute, A. Dereux, E. Devaux, T. Ebbesen, C. Girard, M. U. Gonzalez, and A. L. Baudrion "Near-field characterization of Bragg mirrors engraved in surface plasmon waveguides," Phys. Rev. B **70**, 235406 (2004).
14. R. Köhler, A. Tredicucci, F. Beltram, H. E. Beere, E. H. Linfield, A. G. Davies, D. A. Ritchie, S. Dhillon, and C. Sirtori, "High-performance continuous-wave operation of superlattice terahertz quantum-cascade lasers," Appl. Phys. Lett. **82**, 1518-1520 (2003).
15. N. Finger, W. Schrenk, and E. Gornik, "Analysis of TM-polarized DFB laser structures with metal surface gratings," IEEE J. Quantum Electron. **36**, 780-786 (2000).
16. V. Tamošiūnas, Ž. Kancleris, M. Dagys, R. Simniškis, M. Tamošiūnienė, G. Valušis, G. Strasser and K. Unterrainer "Finite-Difference Time-Domain Simulation of Mid- and Far-Infrared Quantum Cascade Lasers," Act. Phys. Pol. A **107**, 179-183 (2005) and references within.

1. Introduction

Surface plasmons (SP) are transverse-magnetic (TM) electromagnetic waves forming at the surface of materials with negative dielectric constant (like metals below their plasma frequency). They are attracting considerable interest in view of their possible use in the implementation of photonic circuits and subwavelength optics [1]. Recently, they have become the basis for the development of waveguides for quantum cascade (QC) lasers operating in the THz range of the spectrum [2]. In fact, they ideally match the selection rules of intersubband transitions and, more importantly, allow large optical confinement factors to be achieved in relatively thin active regions. THz QC lasers have rapidly developed into high performance devices capable of operating up to 164 K [3] and displaying output powers of up to 200 mW [4]. The first examples of applications have also been appearing, for instance as sources for THz imaging [5, 6] or as local oscillators in heterodyne systems [7, 8].

Recently, single-mode emission has been demonstrated from distributed feedback (DFB) lasers realized with various grating concepts: a combination of etching and selective thermal annealing of the top metal contact [9], resist stripes for loss modulation [10], lateral corrugation of double-metal waveguides [11]. Large grating coupling coefficients have lately been achieved, enabling laser performances similar to Fabry-Perot devices [12]. In this latter case a periodic series of thin slits is opened in the top metallic cladding, carrying the SP waveguide mode.

In the present paper we discuss a different technique, in which the removal of both metal and doped semiconductor prevents the propagation of the surface plasmon mode in the grating slits. A one-dimensional SP photonic crystal is realized, closely corresponding to the concept demonstrated at optical frequencies [13]. The method allows the realization of single-mode THz lasers with as little as 50 grating periods and is used here to demonstrate DFB laser operation in devices without cleaved facets and vertical emission from second-order DFB lasers.

2. Modeling

The design of the active region and the waveguide of our devices are the same as in Ref. [12]. The mode in such a waveguide is a combination of the SPs formed at the bottom contact layer and the SP bound to the metal on top of the active region. Here, we focus on the manipulation of

#70268 - $15.00 USD Received 25 April 2006; revised 31 May 2006; accepted 31 May 2006

the top SP. A way to create a scatterer for this SP is by opening a thin slit in the metal carrying the mode. The slits can then be arranged as a grating of period Λ to act as a one-dimensional photonic crystal, as recently demonstrated by [13]. In a THz QCL, however, the metal is on top of a highly-doped semiconductor layer, usually for the purpose of electrical contacting. This layer also possesses a negative dielectric constant at THz frequencies. Therefore two different ways of fabricating the slits must be distinguished. If the top contact layer is kept continuous below the patterned metal, as in Ref. [12], the SP can still propagate through the slits, traveling at the interface between the highly doped layer and the active region. If, however, this contact layer is also removed in the slits, the SP is suppressed and propagation has to proceed via tunneling through the slits.

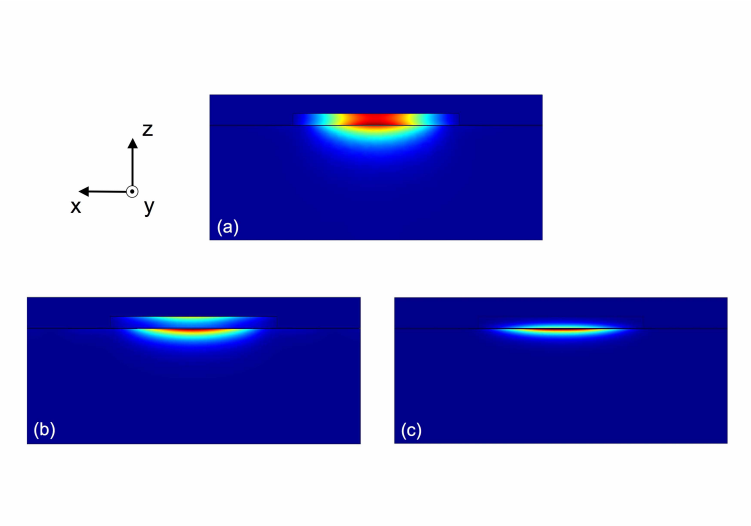

Fig. 1. Computed two-dimensional mode profiles of the considered waveguide configurations. The upper panel (a) shows the fundamental 2.5 THz eigenmode of the standard QCL waveguide described in [12] (see this reference for thicknesses and doping concentrations). The left panel (b) shows the same result for a ridge where the active region is covered by 200 nm of high-doped GaAs, but no metal was deposited. The two different SPs bound to the top and bottom contact layer are clearly distinguishable. The right panel (c) shows the case where the top contact layer was also etched away. The computed losses are α = 9.5 cm^{-1} in (a), α = 105 cm^{-1} in (b), α = 395 cm^{-1} in (c). Note the very high value of the latter configuration; this is due to the mode being tightly bound to the buried layer, close to a frequency singularity of the surface plasmon propagation.

In order to better illustrate the concept, Fig. 1 compares the two waveguide modes which would result in the slit region to the mode of a full standard waveguide. With the highly doped contact layer left in place but no metal, the mode is still partially bound at the top interface, although more closely resembles a combination of two distinct SPs. Without any conducting material on top, the only existing confined mode is strongly bound to the bottom contact layer. These two-dimensional calculations naturally cannot properly depict the real three-dimensional propagation problem as coupling of the SPs across the slits is not considered. Nevertheless they clearly show qualitatively the operating principle. Furthermore, while both approaches are shown to change the spatial distribution of the intensity with respect to the standard complete waveguide and deeply affect the propagation losses, the feedback of a slit without SP is proven to be considerably stronger, as a major spatial mismatch of the modes also arises. In this work, we

#70268 - $15.00 USD Received 25 April 2006; revised 31 May 2006; accepted 31 May 2006

concentrate on the fabrication of such devices in different configurations, expanding the range of possibilities with respect to the simple metallic gratings used in the DFB lasers of Ref. [12]. To estimate the optimum slit width, we computed the reflection from a patterned 400 μm long waveguide. One boundary was excited with an eigenmode of the standard waveguide, and the power flow through the same boundary was plotted as a function of frequency. In order to simplify the problem, only a cross-section formed by the propagation axis y and the growth axis z was considered, and translational invariance was assumed in the perpendicular direction x. This approximates the problem well, as evident also from Fig. 1, because the laser ridge is at least five times larger than the wavelength λ in the material. Figure 2 shows the calculated spectra. For both first ($\Lambda \sim \lambda/2$) and second order ($\Lambda \sim \lambda$) gratings, a slit width of about 2 μm seems to be the best choice, which corresponds to roughly 5 % of the wavelength in the material. This is in agreement to the device properties found in [12], where various gratings were fabricated. As expected, it is also evident from Fig. 2 that the discontinuous top contact layer strongly increases the reflection with respect to the simple metallic grating. Also expected is the lower reflectance of second-order gratings that, for the same wavelength and waveguide length, feature approximately half the number of periods.

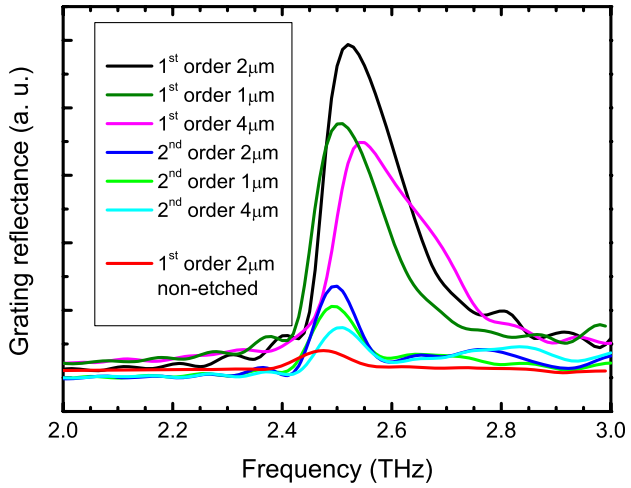

Fig. 2. Finite elements calculation of the reflected power from various SP gratings as a function of the frequency of the waveguide mode. This allows a quantitative comparison of the efficiencies of different grating structures. The red line shows the reflectance from a grating where only the metal layer is discontinuous, and the surface plasmon can still propagate at the highly doped top-contact layer. If this contact layer is also removed by wet etching, the reflectance is considerably increased, as is shown by the black line. The other lines also correspond to etched gratings. For both the first and second order grating, a slit width of 2 μm is the optimum choice. The grating period for first and second order grating are 16.5 μm and 33 μm respectively, the total length of the domain is 400 μm.

3. Fabrication and measurements

The sample was processed into laser ridges, typically 200 - 250 μm wide, by optical lithography, with Ohmic-contact deposition achieved using the procedure described in Ref. [14]. The

#70268 - $15.00 USD Received 25 April 2006; revised 31 May 2006; accepted 31 May 2006

waveguide was completed by the evaporation of Cr/Au on top of the ridges to create the main surface-plasmon interface. This layer was patterned into a series of narrow slits to create the periodic structure for DFB operation or to implement distributed Bragg mirrors (DBR). The fabrication of the slits was carried out by electron-beam lithography using a reduced metal thickness of 100 nm instead of the usual 200 nm to facilitate lift-off. The patterned top metallization was then used as a self-aligned mask to wet-etch the 200 nm top contact layer using a H_3PO_4:H_2O_2:H_2O = 3:1:50 solution. Given the very shallow etch depth, and the small surface area of the slits with respect to total device size, no relevant undercut effect or detrimental influence on the laser transport properties was observed. Devices were then defined by cleaving along a crystal plane and the samples were then soldered to copper bars with an In/Ag alloy, wire bonded, and mounted on the cold finger of a continuous-flow liquid-helium cryostat. Spectra were recorded with a Fourier transform infrared spectrometer in rapid scan mode at the maximum resolution of 0.125 cm^{-1}. Pulsed light-current curves were obtained by collecting the output of one laser facet with f /1 off-axis parabolic optics and focusing it onto a pyroelectric detector, with the whole system contained within the cryostat head to avoid atmospheric absorption.

4. First-order distributed feedback lasers

The strong coupling attainable with the above described SP gratings was first employed for the realization of a first-order DFB device capable of showing single-mode laser action even in a cavity without back facet. Only one edge of the sample was cleaved to define the lasers front

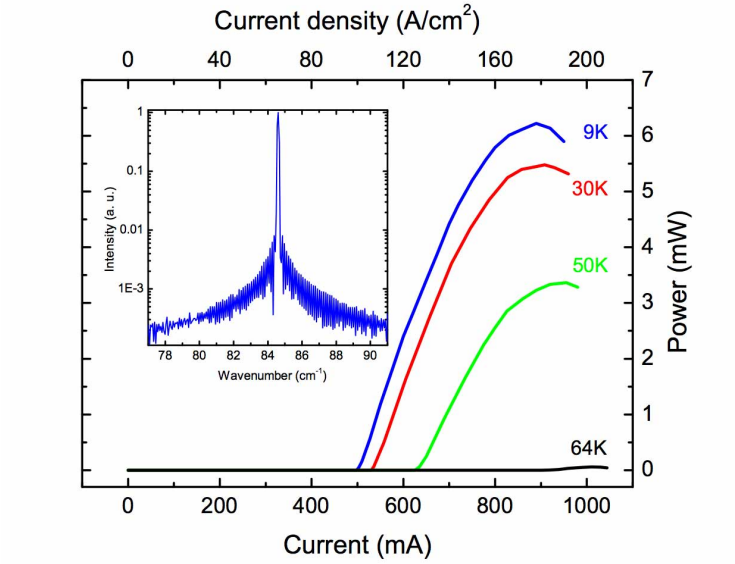

Fig. 3. Light-current characteristics of a 2.5 mm long DFB laser with a grating period of 16.5 μm, collected at various heat sink temperatures. They were measured in pulsed operation at a repetition rate of 400 Hz, using burst of 200 ns pulses for an overall duty-cycle of 5 %. Power calibration was performed at 9 K driving the laser at 50 % duty-cycle. The inset shows an example spectrum recorded at 50 K under an injection current of 0.86 A. The observed laser linewidth is limited by the resolution of the experimental apparatus.

#70268 - $15.00 USD
Received 25 April 2006; revised 31 May 2006; accepted 31 May 2006

facet, while the other uncleaved end of the ridges was left non-metalized and without doped top contact layer, which corresponds to a waveguide with very high losses of the order of 400 cm $^{-1}$ (whose mode profile is shown in the bottom right panel of Fig.1). The reflectivity expected from the end of the metallization is rather small as suggested from calculations with just one wide slit, and confirmed by the absence of lasing in devices without DFB grating. The back facet is then effectively replaced by an absorber at the end of the waveguide, and in this way a resonator consisting mainly of the periodic grating alone is formed. The bonds were then applied along the edge of the ridge, in order to avoid perturbation of the grating.
Figure 3 shows the light-current (L-I) characteristics of a 200 μm wide device with a 2.5 mm long grating. More than 6 mW of peak power are emitted at 9 K, and still over 3 mW are obtained at 50K. Lasing ceases around 65 K. The measured threshold current density of about 100 A/cm^2 is comparable to the one observed in devices with just the metallic grating and two facets [12], demonstrating the effectiveness of this grating scheme in providing the necessary optical feedback. The inset of Fig. 3 shows an exemplary emission spectrum of the same device. A side mode suppression of more than 20 dB is obtained at all investigated injection currents and operating temperatures.

5. Vertical emission from second-order DFB lasers

Lasers were fabricated from a nominally identical re-growth of the structure emitting at 2.5 THz. The same recipes were used, the only changes introduced being the doubling of the grating period, and the use of somewhat broader waveguides (250 - 300 μm). In reality, the gain of the regrown structure is shifted with respect to the previous one, probably due to small variations of the layer thicknesses in the heterostructure, and peaks at slightly lower frequencies between 2.2 THz and 2.3 THz. Therefore proportionally longer grating periods had to be employed. The gratings were limited to a length of 1.5 mm, corresponding to fewer than 50 periods, in the center of the ridge. With devices being 2 mm long, the bonds were then applied

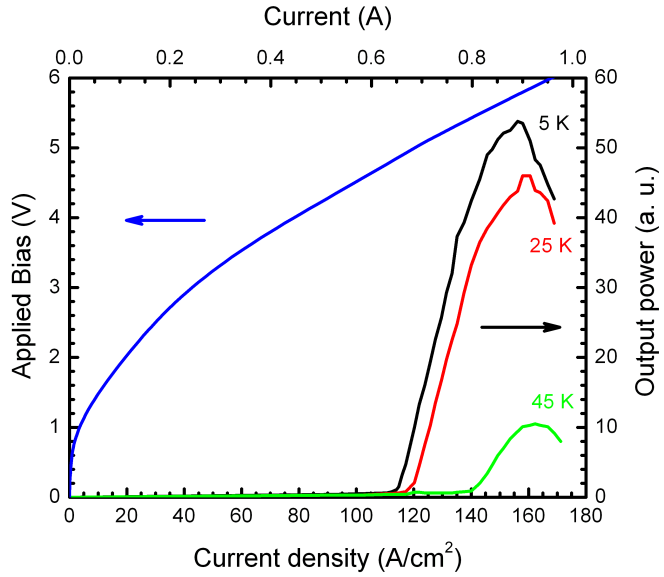

Fig. 4. Vertically emitted power of a 2 mm long and 300 μm wide laser ridge with a grating period of 36.2 μm, recorded at various heat sink temperatures without any collecting lens. The current-voltage characteristics measured at 10 K is also shown.

#70268 - $15.00 USD
Received 25 April 2006; revised 31 May 2006; accepted 31 May 2006

at each end of the ridge, again to avoid perturbation of the grating. Emission spectra were measured both from the facets and perpendicular to the waveguide.
Figure 4 displays the light-current characteristics of the vertical emission collected from one such device. It is rather difficult to estimate the absolute value of the output power in the vertical direction, as the measuring set-up is designed to collect light from a region of space smaller than the grating length. At the same time, also removal of the optics results in a low collection efficiency, owing to the divergence of the beam in the direction perpendicular to the ridge. A rough comparison with the intensity measured collecting the output from the laser facet suggests that the fraction of the emitted light out-coupled vertically by the grating should be about 10 % of the total.

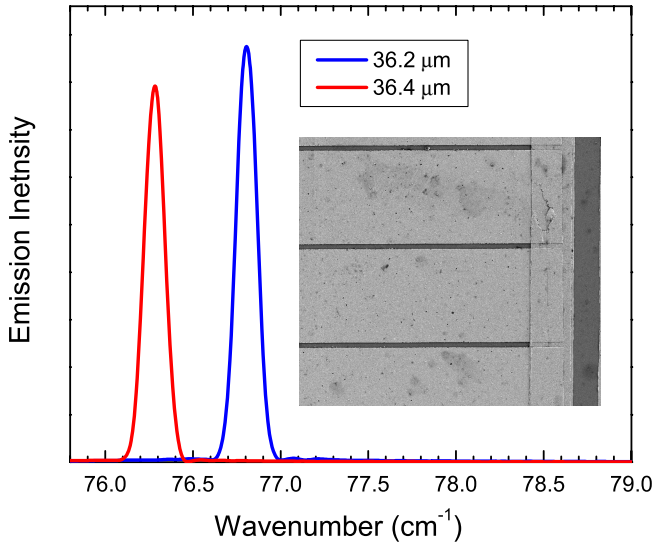

Fig. 5. Laser emission spectra recorded in the vertical direction from two different devices, with 36.2 μm and 36.4 μm gratings respectively. A scanning electron microscope (SEM) picture of the 36.2 μm grating is also reported. On the right the annealed AuGe stripe used for the ohmic contact on top of the laser ridge is clearly visible.

Figure 5 reports two lasing spectra measured from devices with different grating periods. The position of the peaks at 76.3 cm^{-1} and 76.8 cm^{-1} for the 36.4 μm and 36.2 μm gratings respectively is in good agreement with the 76.3 cm^{-1} and 76.7 cm^{-1} predicted using a modal refractive index of 3.6. The correct shift in emission wavelength with grating period and the vertical emission confirm that the grating provides the dominant source of optical feedback. Furthermore, in all the devices measured, lasing was observed on a single *longitudinal* mode. In some of them however, two different *transverse* modes were sometimes detected, which is not surprising in such broad devices, where the first and second transverse mode have nearly equal losses. A slightly higher threshold current density is seen in Fig. 4 with respect to the first-order DFB laser of Fig. 3. This can be partly ascribed to the different sample growth that led to similar small differences also for Fabry-Perot devices. An increase of the optical losses due to the vertically-scattered emission, however, cannot be ruled out.

#70268 - $15.00 USD
Received 25 April 2006; revised 31 May 2006; accepted 31 May 2006

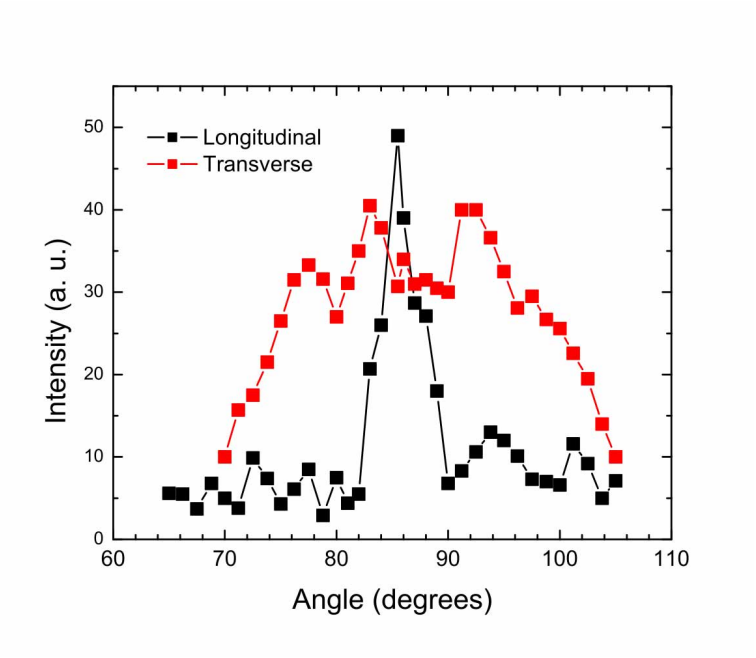

Fig. 6. Angular distribution of the vertical emission from the laser with a grating period of 36.2 μm. The grating extends over 1.5 mm, and the device is 2 mm long and 300 μm wide. As expected, the beam profile is significantly narrower in the direction of the grating. The deviation of the maximum from 90° may be due to the non-perfectly-parallel sample mount inside the cryostat, but may also originate from a slight asymmetric placement of the grating with respect to the laser facets.

Figure 6 shows the vertically emitted power as a function of the angle, both along and perpendicular to the waveguide. As can be seen, the angular distribution along the ridge direction is considerably narrowed, while the transverse beam profile presents a divergence in line with the diffraction due to the lateral size of the ridge. Note that second-order DFB lasers in general, and those using metallic gratings for TM polarization in particular [15], tend to favor operation on an asymmetric longitudinal mode, thereby giving rise to a double-lobe far-field pattern. This feature is not observed in Fig. 6, which is most likely a result of the insufficient angular resolution of the set-up. On the other hand, facet reflection and the ridge sections without grating might also generate phase shifts that result in a nearly symmetric longitudinal profile of the lasing mode.

6. Distributed Bragg reflectors

The same grating concept described above can be used to realize passive functionalities, like for instance distributed Bragg reflectors (DBR), which can be placed at one laser end to enhance facet reflectivity. Note that, in this case, the highly-doped semiconductor layer can be etched away in the whole DBR region before the metal is deposited, as current injection is not fundamental there. To demonstrate the concept we implemented a grating of approximately thirty $\lambda/2$ periods at the back facet of a 2.5 THz Fabry-Perot laser from the same sample of Fig. 3. The L-I characteristics from the front facet are plotted in Fig. 7; powers of more than 13 mW were recorded, the highest value obtained for lasers from this sample.
To test the effectiveness of mirror operation, one should measure the ratio between the output

#70268 - $15.00 USD Received 25 April 2006; revised 31 May 2006; accepted 31 May 2006

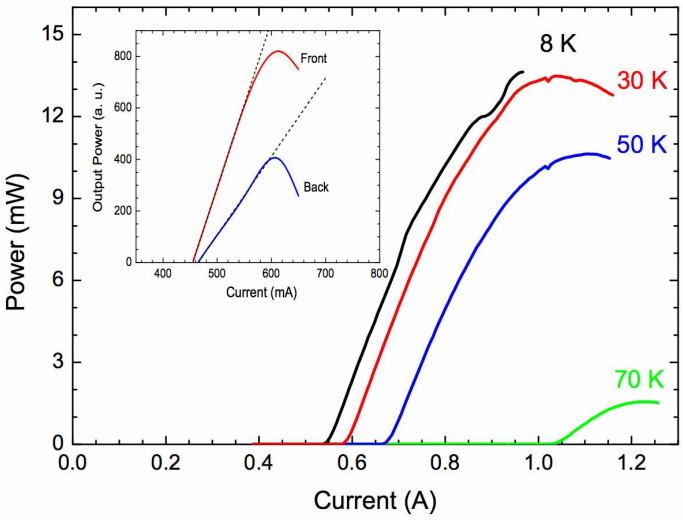

Fig. 7. Output power as a function of drive current for a 2.5 THz QC laser with 16.4 μm period DBR at the back facet. They have been measured in pulsed mode at 5 % duty-cycle, collecting the output from the front facet with f/1 parabolic optics. Inset: L-I characteristics as measured at 8 K from both the front (normal) and back (DBR) facet of a 2.3 THz laser with 18.1 μm period DBR. Linear fits of the slopes are plotted in dashed lines.

intensity emitted from the normal and the DBR facet. In the case of the 2.5 THz device of Fig. 7 a value of about 10 is indeed found. These measurements, however, are quite sensitive to the quality of the facets, as imperfections may result from the cleaving process or in the laser mounting, especially since the waveguide mode extends considerably in the substrate. Such defects can easily lead to under- or over-estimates of the DBR effect. Furthermore, the multi-mode character of Fabry-Perot devices can complicate the analysis, since different longitudinal modes can experience very different DBR reflectance, owing to its limited bandwidth. For the same reason, the DBR period has to precisely match the wavelength of maximum gain to be significantly effective. We have thus decided to perform a more careful study, using this time a 2.3 THz sample, making sure to employ devices with high quality of both facets, and to correlate power and spectral measurements. The highest front-to-back intensity ratios were found for 18.1 μm period DBRs, where values slightly larger than 2 were obtained. The inset of Fig. 7 reports the respective L-I curves as measured at 8 K for an exemplary device. From the fit of the slope efficiency dP/dI in the two cases, one can easily derive a relation between the front and back facet reflectance R_F and R_B, by noting that:

$$\frac{(dp/dI)_F}{(dp/dI)_B} = \frac{\ln R_F}{\ln R_B}. \tag{1}$$

Assuming R_F is 0.32 as computed from Fresnel formula for a modal refractive index of 3.6, we then get from the fit R_B = 0.58. This value might be slightly underestimated, as minor asymmetries in power measurements were often found with Fabry-Perot devices, probably owing to a non-perfect cryostat mount. In any case, while clearly larger than R_F, the magnitude of R_B also suggests that DBRs somewhat longer than 30 periods are necessary to constitute a

#70268 - $15.00 USD Received 25 April 2006; revised 31 May 2006; accepted 31 May 2006

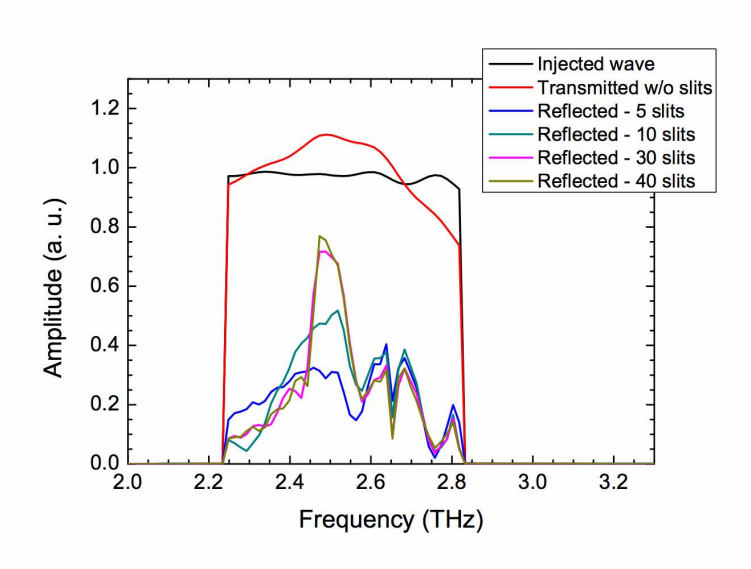

Fig. 8. FDTD calculation of the grating effect on mode propagation within the 2.5 THz laser waveguide. The amplitudes of the magnetic field component H_y recorded during the FDTD simulation are displayed. In black we report the spectrum of the injected wave, in red the amplitude of the transmitted wave after 1030 μm of propagation in an unstructured waveguide. The other curves display the amplitude of the reflected wave for a varying number of grating slits.

reasonable alternative to high-reflection coatings. To get a quantitative understanding of these numbers, the Finite-Difference Time-Domain (FDTD) method with additional modules [16] was employed to model the propagation within the waveguide with a grating segment. Initially, a regular Fabry-Perot waveguide with ideally reflecting facets was simulated in order to obtain the intensity distributions for different mode numbers and frequencies. Afterwards, the distributions and phase information obtained during the previous step for the 2.25 - 2.82 THz range were employed for simulating the "hard source" at the end of a 257 μm long waveguide. So-called "absorbing boundary conditions" were specified for the second end of the waveguide and, therefore, effectively only one-way propagation was modeled during this part of the investigation. Electric and magnetic field components were recorded near the absorbing end of the waveguide during each step of simulation and used for the simulation of the waveguide with grating, which was run in parallel.

Results depicted in Fig. 8 were obtained for a 1030 μm long waveguide with different numbers of slits. The entire simulation region was split into two, so-called "total-field" and "reflected-field," ones. Field values from the second program were used to simulate the transparent source of the incident wave at the boundary between the two regions. Both ends of the waveguide were made "absorbing" in this case, in order to avoid the additional reflections. In all cases, the DBR was placed 206 μm away from the beginning of the simulation region, while a peak gain of 20 cm^{-1} with a 2.5 meV full-width-at-half-maximum was considered for the active region in order to better represent the actual device, operating slightly above the waveguide losses. The amplitudes of the incident wave were recorded at a distance of 51.5 μm from the beginning of the simulation region.

As expected, a sharp reflectivity peak at the Bragg frequency builds up when increasing the number of grating slits. At this point, the amplitude of the reflected wave for 30 slits is ap-

#70268 - $15.00 USD Received 25 April 2006; revised 31 May 2006; accepted 31 May 2006

proximately equal to 70 % of the incident wave amplitude, which translates into approximately 50 % of the intensity of the incident wave. Such prediction is consistent with our experimental data, and even more so when the increase due the refractive index mismatch with air at the facet is taken into account. This could push the reflectance up to about 65 %, depending on the phase. Note also the relatively narrow DBR working range of less than 100 GHz. As previously discussed, this requires a precise choice of grating period for proper operation. As an example in fact, we also measured 2.3 THz lasers with 17.9 μm period DBRs; they displayed a ratio between the front and back slope efficiencies of about 1.3, translating into a smaller reflectance $R_B = 0.42$. Additional features result in the simulation away from the main maximum. They can be attributed to the influence of the excited higher order modes in the vicinity of the grating.

7. Conclusion

We have presented a technique to structure and significantly alter the propagation of the surface plasmon mode forming at the metal interface in the waveguide of THz QC lasers. For the purpose, the stack of top contact layer and metal, which carry the surface plasmon, were periodically interrupted by thin slits that act as barriers for the surface plasmon propagation. Arranged in a periodic, one-dimensional photonic crystal, a series of such slits provides stronger coupling coefficients than previously demonstrated with other distributed feedback concepts. As applications, high-performance first-order THz DFB lasers were realized, in which back facet reflectivity was suppressed by inserting an absorbing section. Second-order DFB devices, where the single-mode THz laser radiation was shown to be vertically emitted, were also fabricated, with as little as 50 grating periods. The use of this method for the implementation of DBRs at the laser back facet was finally investigated.
We believe the technique here proposed can be easily exploited in the near future for the realization of two-dimensional THz photonic crystal devices. Furthermore it should allow the development of vertically-emitting DFB lasers with circular geometries, which would offer the relevant advantage of symmetric and better collimated beam profiles.

Acknowledgments

This work was supported in part by the European Commission through the IST integrated project “Teranova”, the PASR “Terasec”, and the Marie Curie RTN “Poise”. Partial financial support of the Scuola Normale Superiore from Physical Sciences Inc. is also gratefully acknowledged.

#70268 - $15.00 USD Received 25 April 2006; revised 31 May 2006; accepted 31 May 2006